DISCRETE DYNAMICS AND EPIDEMIOLOGICAL MULTI-PHYSICS MODELS FOR TRANSPORTATION

FINAL REPORT

JUNE 2021

SIRISH NAMILAE & DAHAI LIU

US DEPARTMENT OF TRANSPORTATION GRANT 69A3551747125

DISCLAIMER

The contents of this report reflect the views of the authors, who are responsible for the facts and the accuracy of the information presented herein. This document is disseminated under the sponsorship of the Department of Transportation, University Transportation Centers Program, in the interest of information exchange. The U.S. Government assumes no liability for the contents or use thereof.

1. Report No.	2. Government Accession No.	3. Recipient's Catalog No.
4. Title and Subtitle Discrete Dynamics and Epidemiological Multi-Physics Models for Transportation		5. Report Date JUNE 2021 6. Source Organization Code
7. Author(s) SIRISH NAMILAE AND DAHAI LIU		8. Source Organization Report No. CATM-2021-R4-ERAU
9. Performing Organization Name and Address Center for Advanced Transportation Mobility Transportation Institute 1601 E. Market Street Greensboro, NC 27411		10. Work Unit No. (TRAIS) 11. Contract or Grant No. 69A3551747125
12. Sponsoring Agency Name and Address University Transportation Centers Program (RDT-30) Office of the Secretary of Transportation–Research U.S. Department of Transportation 1200 New Jersey Avenue, SE Washington, DC 20590-0001		13. Type of Report and Period Covered Final Report: FEB 2019-JUNE 2020 14. Sponsoring Agency Code USDOT/OST-R/CATM
15. Supplementary Notes:		

16. Abstract

Air transportation is central to the global mobility of goods and people. Elimination or reduction of air travel during epidemic emergencies, such as during the 2014 Ebola outbreak in West Africa, carry considerable economic and human costs. This has come to the fore in the current COVID-19 crisis. Air travel has been identified as a leading factor in the spread of several epidemic diseases including influenza, SARS, as well as COVID-19. Mathematical modeling can play a crucial role in understanding this problem and devising strategies to mitigate emergency transportation disruptions. There is a strong correlation between contact rates and infection rates in a number of disease epidemics. The mixing of susceptible and infectious individuals in these high people density locations like airports involves pedestrian movement, which needs to be taken into account in the modeling studies of disease dynamics. Understanding the evolution of pedestrian contact network and designing strategies for epidemic mitigation can only be achieved by accurate modeling of pedestrian movement trajectories, and interactions as individuals move through crowded built environments like airports. In this project, a social force based pedestrian dynamics approach is used to evaluate the contacts among proximate pedestrians, which are then integrated with a stochastic epidemiological model to estimate the infectious disease spread in a localized outbreak. Practical application of such multiscale models to real life scenarios can be limited by the uncertainty in human behavior, lack of data during early stage epidemics and inherent stochasticity in the problem. We address this problem in two ways: (a) Firstly, we use other data sources such as airport usage data and cell phone location based data to estimate the number of people in crowded locations. The pedestrian dynamics simulations with the data input are more reliable. (b) Secondly, we parametrize the sources of uncertainty and explore the associated parameter space using a novel high-efficiency parameter sweep algorithms. Results point to the effectiveness of this modeling approach and the algorithmic developments

<table>
<tr><td colspan="2">17. Key Words
Pedestrian Dynamics, Epidemic model, Parameter Sweep</td><td colspan="2">18. Distribution Statement
Unrestricted; Document is available to the public through the National Technical Information Service; Springfield, VT.</td></tr>
<tr><td>19. Security Classif. (of this report)
Unclassified</td><td>20. Security Classif. (of this page)
Unclassified</td><td>21. No. of Pages
49</td><td>22. Price
…</td></tr>
</table>

Form DOT F 1700.7 (8-72) Reproduction of completed page authorized

TABLE OF CONTENTS

EXECUTIVE SUMMARY

Reducing the interactions between pedestrians in crowded environments can potentially curb the spread of infectious diseases including COVID-19. The mixing of susceptible and infectious individuals in many high-density man-made environments such as waiting queues involves pedestrian movement, which is generally not taken into account in modeling studies of disease dynamics. In this project, a social force based pedestrian dynamics approach is used to evaluate the contacts among proximate pedestrians which are then integrated with a stochastic epidemiological model to estimate the infectious disease spread in a localized outbreak.

Practical application of such multiscale models to real life scenarios can be limited by the uncertainty in human behavior, lack of data during early stage epidemics and inherent stochasticity in the problem. We address this problem in two ways: (a) Firstly, we use other data sources such as airport usage data and cell phone location based data to estimate the number of people in crowded locations. The pedestrian dynamics simulations with the data input are more reliable. (b) Secondly, we parametrize the sources of uncertainty and explore the associated parameter space using a novel high-efficiency low discrepancy sequence (LDS) parameter sweep algorithm.

We show the effectiveness of these two approaches in improving the model outcomes. In particular the low discrepancy sequence (LDS) parameter sweep is effective in reducing the number of simulations required for effective parameter space exploration in this multiscale problem. The algorithms are applied to a model problem of infectious disease spread in a pedestrian queue similar to that at an airport security check point. We utilize

Orlando International airport as a modeling test-bed for the simulations. The primary outcomes of this research include the following: (a) Pedestrian movement layouts in high density areas like airport security queues can impact infectious disease spread. (b) Novel data sources like cellphone based data can provide an effective means for reducing the uncertainty associated pedestrian dynamics modeling. (c) We find that utilizing the low discrepancy sequence based parameter sweep, even for one component of the multiscale model reduces the computational requirement by an order of magnitude

1. INTRODUCTION

Computational models play a key role during pandemics by enabling the exploration of different "what if" scenarios for planning public health interventions. Most common infectious disease models however focus on large populations at the scale of large geographic regions. Unlike models that evaluate the disease spread dynamics using demographic or environmental conditions, contact based models directly relate the disease transmission to the contact network. Computational models of smaller local outbreaks that incorporate proximate contacts have been used to correlate fine scale human interventional behavior to disease transmission (Heesterbeek *et al*., 2015). For example, such analysis during the 2017 Ebola outbreak helped assess transmission and preventative strategies for specific settings such as funerals (Merler *et al*, 2015) and airplanes (Namilae *et al*, 2017). Analysis of the heterogeneous mixing patterns in epidemiological modeling facilitates a better understanding of the disease dynamics (Barrat *et al*., 2010). Ignoring the heterogeneity in the contact network may lead to inaccurate results (Smieszek *et al*, 2009). While researchers have developed models that incorporate contact data through contact tracing data (Smieszek *et al* , 2009) and survey data (De Cao *et al*, 2014), the spread of COVID-19 poses unique challenges. There is direct evidence for the spread of COVID-19 clusters in various high-people density locations with variations of above factors, including shopping malls (Cai *et al*, 2020), concerts (Nippon, 2020), nursing homes (LA Times, 2020), cruise ships (Mizumuto, 2020), churches (WSJ, 2020) and mass gatherings (Xu *et al*, 2020). These reports suggest that colocation and movement of people in a crowded location even over relatively short periods leads to the

disease spread. Pedestrian movement modeling can provide possible trajectories of pedestrians that can be used to model contact heterogeneity in crowded locations mentioned above.

Among the various pedestrian movement models, e.g. cellular automata (Burstedde,2001), fluid flow (Henderson, 1971) and queuing (Okazaki and Matsushita, 1993), social force models (Helbing et al 1995, 2000) are most suited for individual trajectory evolution, required for contact estimation. Social force models first proposed by Helbing and Molnar (1995) extend the concepts of force balance from molecular dynamics to pedestrian movement. Here, the forces are a measure of the internal motivations of individual pedestrians to move towards their destination in presence of obstructions like other pedestrians and objects. Social force models have been applied to crowd simulations situations in panic (Helbing *et al*, 2000), traffic dynamics (Treiber *et al*, 1999), evacuation (Wei-Guo *et al*, 2006 & Helbing *et al*., 2002) and animal herding (Li *et al*, 2014). Algorithmic developments have included generation of force fields using visual analysis of crowd flows (Mehran *et al*, 2009), explicit collision prediction (Zanlungo *et al*, 2011), and collision avoidance (Lämmel *et al*, 2012). Namilae *et al*. (2017a & 2017b, 2020) have combined pedestrian dynamics and stochastic epidemic models to study the spread of infectious diseases in settings like airplanes and pedestrian queues.

Airborne diseases including COVID-19 are spread when susceptible individuals inhale pathogens suspended in the air. These organic particles are secreted by the nasal tracts and throat of an infected individual and are dispersed to the environment through expiratory events including breathing, talking, sneezing or coughing. As these viral particles are able to remain suspended in the air and navigate distances of several feet, there is a high risk of disease

outbreak in a local area with high density of people. Several factors determine the extent of transmission that will take place between the infective and the susceptible population; these include (1) the infectivity of the contagion, (2) survival lifetime of the pathogen, (3) the environmental conditions like the temperature and airflow that determine the contagion spread, (4) the extent of mixing between susceptible and infectious individuals resulting in new contacts and (5) the duration of the contacts. The parametric range associated with each of these factors and the diversity in the initial conditions and the locations of potential disease spread exacerbate the prediction problem.

This uncertainty can be addressed in two ways. Models that incorporate empirical data can reduce the uncertainity. For example, new data sources like cell phone location data, twitter geotags etc can provide details of pedestrian numbers and paths which can be input to the pedestrian dynamics models. Despite this there is uncertainity associated with the large number of stochastic parameters in the models. This can be addressed using parameter sweep algorithms and parallel computing. Parameter sweep is an important computational tool that employs parallel computing resources to execute multiple computations with different combinations of values of the same parameters. Large-scale parameter sweep runs have found extensive applications in many scientific and engineering fields (Youn & Kaiser, 2010). For example, parameter sweeps have been used to model electromagnetic cascade showers (Nelson *et al*, 1985), photochemical pollution (Abramson 1994), stratospheric warming events (Naito *et al*, 2003), high energy physics applications (Basney *et al*, 2000), etc. Chunduri *et al* (2018) used a Low Discrepancy Sequences based scrambled Halton sequence to effectively reduce the parameter space for a pedestrian dynamics based contact estimation problem. Here we

extend this approach to address the parameter space in the multiscale pedestrian-dynamics infection spread problem.

The objective of this research is to evaluate the effect of pedestrian movement in airports on the spread of infectious diseases. We utilize a social force based pedestrian dynamics model using in-house codes and Anylogic agent based modeling software, and integrate it with a stochastic infection dynamics model to analyse the spread of infectious disease in crowded areas in the airports. Novel data sources are used to identify the high people density regions in the airport, which are modeled using pedestrian dynamics. There are several parameters with inherent uncertainties in both pedestrian dynamics and infection spread models. In order to comprehensively understand this problem, the infectious disease spread needs to be investigated for various combinations of the parameters. Here, we show that a parameter sweep algorithm based on low discrepancy sequence can be extremely effective in reducing the parameter space for this multiscale problem.

2. MULTISCALE MODELING APPROACH

This computational model addresses the transmission and dispersion of fatal infectious pathogens in locations, where large groups of people gather at high densities, through a multiscale model that combines pedestrian dynamics with stochastic infection spread models. The pedestrian dynamics models uses a Molecular Dynamics (MD) based numerical approach called social force method. The MD algorithm captures the step-by-step evolution of the system of particles tracing their trajectories and can be used to estimate the contact frequency between passengers during air-travel. We incorporate this contact analysis into a discrete-time stochastic Susceptible-Infected (SI) model with infection probability and contact radius as primary inputs. This generic model is applicable to several directly transmitted diseases including COVID-19 by varying the input parameters, and can be used to assess the influence of pedestrian movement on disease spread. This multiscale framework is used to analyze the infectious disease spread in a winding queue configuration under various transmission scenarios using a parameter sweep.

2.1. Pedestrian dynamics using social force model

In the context of modeling the pedestrian mixing patterns to analyze infection spread in crowded environments, numerical simulations are performed to mimic the movement behavior of pedestrians. Here, the pedestrians are considered to be particles whose motion is determined by a balance of repulsive and propelling forces. The resulting trajectories are used to estimate the number of contacts. The repulsive ($\vec{f}_i^{ped}$) and attractive ($\vec{f}_i^{int}$) forces are summated as in as in Namilae *et al*. (2017a & 2017b). The tendency to avoid collision and

impenetrability with other individuals in high density crowds and immobile obstacles in the pedestrian's path are represented by the repulsive terms.

$$\vec{f}_i^{ped} = \sum_{i \neq l} \vec{\nabla}\, \varphi(r_{il}) = \sum_{i \neq l} \vec{\nabla}\, [\, \epsilon\, (\frac{\sigma}{r_{il}})^{12}] \tag{1}$$

Where ϵ and σ are repulsive force field parameters and r_{il} is the distance between the i^{th} and the l^{th} nearest front pedestrian in the queue. On the other hand, pedestrian self-propulsion to their target destination (e.g. an exit) either individually or collectively results in another force. This intention force is obtained by the average rate of change of momentum:

$$\vec{f}_i^{int} = \frac{\overrightarrow{\Delta P}}{\tau} = \frac{1}{\tau} \left[\vec{P}_{0i}(t) - \vec{P}_i(t)\right] \tag{2}$$

Pedestrians move at the speed of the nearest person ahead in a queue. This is accounted for by the location dependent- desired velocity, in the direction of motion $\hat{e}_1$, in the self-propulsion term as:

$$\vec{P}_{0i}(t) = m_i v_0^i(t)\, \hat{e}_1 = m_i \begin{cases} (v_A + \gamma_i v_B) \left(1 - \frac{\delta}{\min\{r_{ij|_{front}}\, ; i \neq j\}}\right) \hat{e}_1 \\ 0\, ; if\ r_{ij|_{front}} < \delta \end{cases} \tag{3}$$

$$\text{Where } \delta = \begin{cases} \delta_1\, ; if\ i\ \&\ j\ of\ same\ group \\ \delta_2\, ; if\ i\ \&\ j\ of\ different\ groups \end{cases}$$

The proposed social force model allows evolution of the pedestrian in time domain. The number of contacts is then obtained from the generated trajectories. The contact data is utilized in an epidemiological model to map the infectious disease propagation in the population.

2.2. Pedestrian dynamics using Anylogic - agent based modeling

The model mentioned in the previous section is developed in house as a FORTRAN program and is especially useful for running large number of simulations using parallel

computing. However, the layouts needed for the simulation need to be manually generated, which leads to some limitations when modeling complex geometries. We use Anylogic Agent based modeling software to overcome some of these limitations for complex geometries and layouts. The larger scale model at the level of entire airport is created using Anylogic. Detailed model of a given section is then developed using in-house codes for parallel implementation and parameter sweeps. Note that infectious disease modeling requires pedestrian trajectories only and can work with either pedestrian dynamics model.

We develop a simulation model of pedestrian movement in Orlando International Airport (MCO) by incorporating the social force model in agent-based simulation software AnyLogic. The layout of the second floor of the MCO modeled to scale is shown in figure 1. Pedestrians enter through the entry line (target line) and go to the waiting area. There are three waiting areas (food court & lounges) in the model, they were drawn using polygonal node under space markup. Service with lines component is used to outline the security check-in. West zone security check-in has four services and one queue, east zone large aisle has two services with a single queue, similarly east zone small aisle has two services and a queue. For airport security check-in areas serpentine lines are used as a queue. The blocks in the pedestrian library are used to construct flow charts that help to generate, control, and process pedestrians in the model.

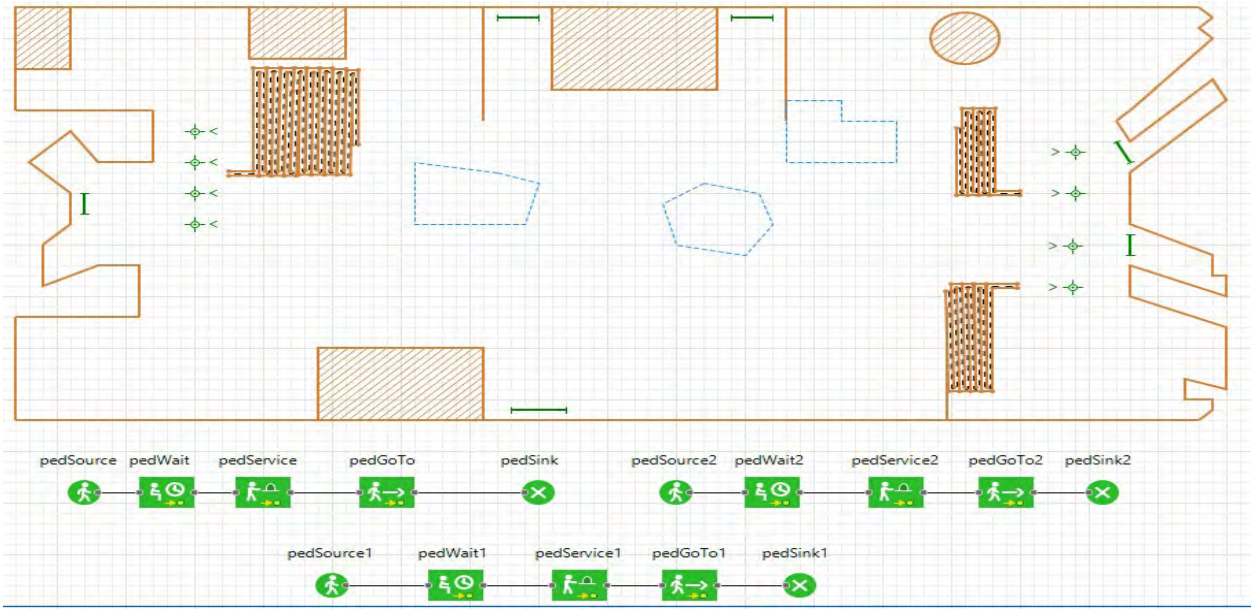

Figure 1. Anylogic model of the Orlando international airport and associated flowcharts.

The model has three separate flow charts to represent three entry and exit points. The first block is pedSource which generates pedestrian arrival. We set the number of pedestrians and limit the number of arrivals as required for each entry points, 600 pedestrians are used for the west zone and 300 each for east zone aisles. Once the pedestrians enter the airport, they will first enter into waiting areas, as modeled by pedWait block. It allows pedestrians to wait for a specified time in particular area to simulate pedestrian activities before the check-in process . After the waiting, pedestrians enter into pedService block which simulates the security check-in process, in which they wait in a single queue to be serviced. After check-in services, pedestrians will walk to their specified targets, simulated by pedGoto block. By using pedGoto, pedestrians find a path to the specified destination. Finally, pedSink is used to simulate that a pedestrians that leave the airport which is the endpoint for pedestrian flow.

The input for the number of pedestrians in the different regions of the airports is based on cellphone location data. The individual blocks at the security check are modeled in detail using the in-house codes for the parallel parametric sweep and the infection spread analysis.

2.3. Epidemiological model

Consider a population of size N consisting of I(t) infected and S(t) susceptibles at time t. A susceptible can become infected when coming into direct contact with an infected. Given the trajectory of pedestrians over time, the number of contacts m_i can be evaluated as:

$$m_i(t) = \sum_j r_{ij}.\lambda_{ij}, \quad \text{where } \lambda_{ij} = 0 \text{ if } r_{ij} > x \text{ and } \lambda_{ij} = \frac{1}{r_{ij}} \text{ if } r_{ij} < x \tag{4}$$

Here, r_{ij} is the distance between *i* and *j* pedestrians and *x* is a virus specific distance parameter. Pedestrian position ($r_i(t)$) evolves through pedestrian dynamics and is a function of the age, sex and infection status.

The transmission distance (x) used to define the contact is dependent on the type of pathogen and mechanisms for its spread. For diseases like Ebola, studies indicate that primary mode of transmission is through contact droplets (Osterholm 2015, Judson 2015, Nikiforuk 2017). Consequently, a distance that enables direct touch needs to be used for estimating contacts for such diseases. Other infectious diseases like SARS are known to be transmitted by both shorter and longer range airborne mechanisms (Clark 2009, Li 2004). Likewise, the influenza can be transmitted through coarse droplets or microscale bioaerosols being respired into the respiratory tract of a susceptible individual (Yuen 2005). Studies suggest that transmission occurs when the virus particles are suspended in air and inhaled by a susceptible individual or when that individual touches a contaminated surface with deposited droplets and

then touches their eyes, nose or mouth (Yuen 2005). The size of these particles can play an important role in contagion dispersion. Small particles dispersed in aerosols transmit over large distances. For example, experiments indicate micrometer sized aerosol clouds generated during cough traveling over 2 m (Bourubia 2014, Gupta 2009).

Consider that the infection spread initiates due to the insertion of i_c^0 infectives initially (t_0= 0) at their "c" days of infection, out of "d" incubation days. Denote by P_{inf} the probability that a contact between a susceptible and an infective (or contaminated surface) results in infection of the susceptible. We divide this input parameter into two components: a viral shedding probability distribution (P_c) which is a function of time since acquiring infection for specific virus in question, and a pathogen spread mechanism component (P_m). This includes contributions of several independent mechanisms comprising (a) aerosol exposure and inhalation probability (P_a) common in infections such as Norovirus (Friesema, 2009) and Ebola Jaax(1995), (b) Coarse pathogen droplet inoculation (P_d) common in influenza and SARS (Mangli 2005). COVID-19 transmission is primarily driven by proximity between an infective person and a susceptible person, and can be transmitted by both aerosol and close contact mechanisms (CDC 2021). Other mechanisms including fomite mechanism, which involves contaminated surface-to-hand transfer would contribute to the infection spread, but such mechanisms do not involve human-to-human contact in this context. The infection probability would then be defined as:

$$P_{\text{inf}} = P_c.P_m = P_c\left(P_a + P_d\right) \qquad (5)$$

Consider the viral shedding probability distribution (P_c). Studies indicate that the amount of viral shedding is typically dependent on the days post symptom appearance for the infected

individual and the length of incubation period. In a previous study (Namilae 2017 a&b), we used CDC data on amount of RNA (ribonucleic acid) virus copies in the blood serum since the illness contraction to generate this probability distribution for Ebola in Figure 2.a (Towner 2004). Similar approach can be used for other diseases, for example, for SARS pathogen (Figure 2.b), the viral gene expression of the nucleocapsid (N) protein, detected at different rates along the evolution of the virus from post onset of the symptoms till convalescence is indicative of viral shedding and can be used to generate the P_c distribution (Zhao 2007). For influenza, nasal, oral or ocular shedding of H1N1 virus has been detected by determining the relative equivalent unit (REU) from viral RNA level (Paquette 2015). Such data can be used to generate the P_c distribution (Figure 1.c). Figure 1 shows the viral shedding distributions we generated based on viral shedding for H1N1 influenza and SARS respectively. While we consider maximum infectivity for calculating term incorporates the differences in infectivity due to variations in infectious individuals. The stochasticity in individual's susceptibility is accounted for via the binomial or Poisson distribution.

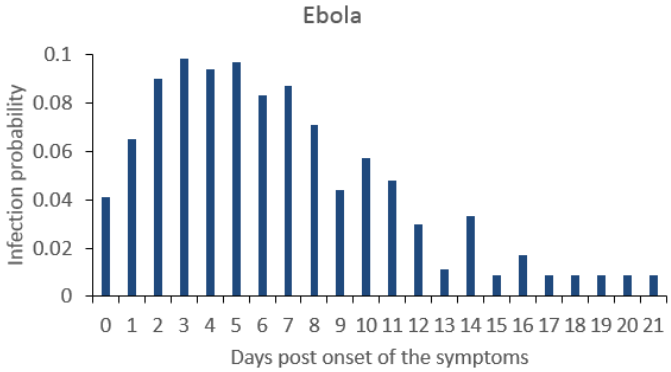

(a)

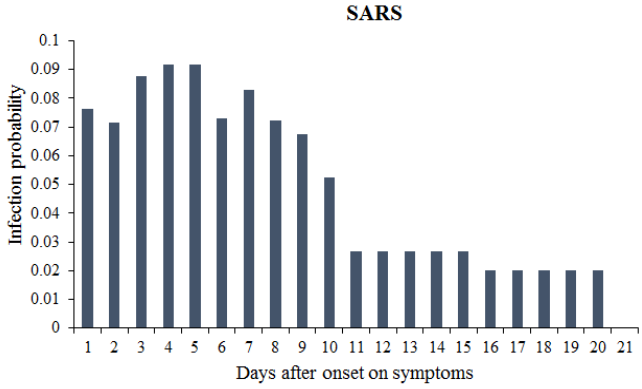

(b)

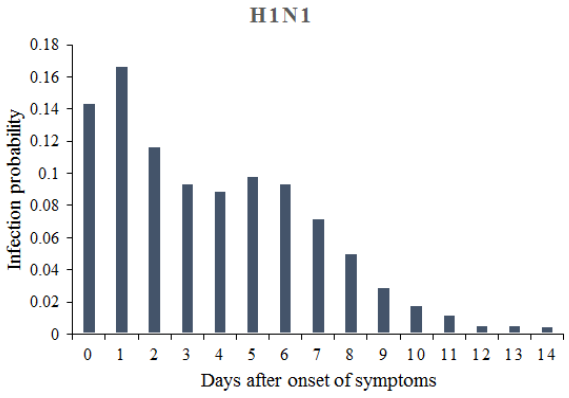

(c)

Figure 2 Infectivity probability distributions (Pc) (a) along the days after clinical signs of Ebola infection, (b) during viral shedding of SARS and (c) H1N1

The distribution of the infective individuals in the crowd is unidentified; any of these pedestrians can be probably infective. We assume that the infectives can be in anywhere among the crowd, so there are many possible permutation patterns of infectives location within the crowd. Denote by "Comb" the possible permutations of infectives which depend on the assumed number of infectives and the total number of the population. All these possible permutations are run successively, and at each run the number of susceptible individuals $S_i(t-1)$ in contact with the infectives is counted. Then, the number of newly infected individuals is a binomial distribution of the number of individuals in contact $S_i(t-1)$ and probability of success of viral transmission p_i. Repeating the same process for all the infectives with different days of infection c and at different locations in the crowd, further binomial distributions are obtained. Denote by λ the possible number of newly infected pedestrians ranging from zero to the maximum obtained number N_{inf} (λ= 0,…,λ_i,…,N_{inf}). Also let w_i be the frequency of obtaining the same λ_i in the runs. In order to obtain the mean binomial distribution of the number of people infected at time t by all of the infectives with varying age of infection "c", we combine the probability plots and average them as given by:

$$I(t) \sim \sum_{c=1}^{d} \sum_{i=1}^{i_c^0} \{Binomial\ [S_i(t-1), P_m . P_c\ \frac{m_i(t-1)}{N}]\}^* w_i\ (\lambda_i) / C \qquad (6)$$

Where $w_i\ (\lambda_i)$ is the frequency of the mean λ_i repetition during all the possible combinations "C" of infectives. Note that the contacts are defined when pedestrians are within a specific transmission distance which is dependent on the transmission mechanism. Instead of using fixed parameters for defining contact, we will treat contact distance and contact definition as one of the parameters in assessing epidemic spread and vary it over the parameter space to mimic epidemic dispersion in different conditions, within the various pedestrian dynamics

configurations associated with winding queues. Based on the above discussion, we vary the contact distance between 2.1 m and 0.9 m which are representative of aerosol and coarse droplet mechanisms respectively. Similarly, the infection probability (P_{inf}) is varied as a parameter up to a value of 0.2 to represent various levels of infectivity.

The Binomial distribution is valid for a large crowd with higher probability of infection. This applies to the winding queues. However, in the situation where N is large and P_{inf} is very small (below 0.1), for instance during boarding and deplaning, the Poisson distribution can be used to approximate the binomial distribution. Here, I(t) is distributed using the Poisson approximation:

$$\mathrm{I(t)} \sim \sum_{c=1}^{d} \sum_{i=1}^{i_c^0} \{Poisson\,[S_i(t-1), P_m . P_c\ \tfrac{\mathrm{m_i(t-1)}}{N}]\}^{*}\ w_i\ (\lambda_i)\ /\ \mathrm{C} \qquad (7)$$

The infection probability, radius of infection and pedestrian dynamics model parameters are all considered to be parametric variables. By varying these parameters over the space of possible numerical values, one can analyze how mitigation measures related to pedestrian movement would impact the disease spread in a wide variety of conditions. This makes the approach generic and applicable to new diseases like COVID-19 by varying the parameterization. However, given the extremely large parameter space, efficient algorithms are desired to cover the parameter space effectively.

The contact data is obtained from pedestrian trajectories by comparing the distance between pedestrians to the transmission threshold (x) dependent on the types of pathogen and mechanisms for its spread.

The infection probability, radius of infection and pedestrian dynamics model parameters are all considered to be parametric variables. By varying these parameters over the

space of possible numerical values, one can analyze how mitigation measures related to pedestrian movement would impact the disease spread in a wide variety of conditions. However, given the extremely large parameter space, efficient algorithms are desired to cover the parameter space effectively.

2.4. Parameter Sweep Methods

Parameter sweep algorithms are used to efficiently cover the parameter space and account for combination of the parameters that significantly affect the model outcome. A conventional parameter sweep approach is lattice based method wherein the parameters are uniformly partitioned. For example, consider a two-dimensional parameter space; in the lattice parameter sweep, the points (or parameters values) in the horizontal and vertical directions are equally spaced respectively. This scheme is inefficient in terms of domain coverage and for checking convergence (Chunduri *et al*, 2018). For example, consider a situation where the model has d parameters resulting in a d-dimensional parameter space. If this is partitioned uniformly in these dimensions with R points (representing simulations) for each parameter, the total number of points obtained is $N = R^d$. In order to check for convergence, if we refine the space domain by doubling the number of points. Then, the number of points N' becomes, $N' = R'^d = (2R)^d = 2^d R^d = 2^d N$. This ratio between the two consecutive lattice sizes ($\Delta N = 2^d$) is very large and is imprecise for checking convergence. Also, running a simulation of N' grid points is computationally exhaustive and time consuming. Instead, alternate non-uniform parameter sweep techniques offer better convergence and faster outcomes.

Non-uniform domain partition methods based on the pseudo-random and quasi-random sequences are promising algorithms for nodes sequence generation enabling faster

convergence at lower number of nodes compared to the lattice method. These methods are commonly used in Monte Carlo and quasi-Monte Carlo algorithms to solve for numerical integration problems (Radovic 1996). In a Monte Carlo simulation, the accuracy of the results depends on the generation of the pseudorandom sequence over a [0,1] interval. Using a random sequence was found to be asymptotically slower than LDS because sparse and clustered regions are observed in the space domain (Chunduri *et al* 2018).

Quasi-random sequences are deterministic alternatives to pseudo-random sequences. They are infinite sequence of points, used in Quasi-Monte Carlo (QMC) simulations (Morokoff & Caflisch, 1994). These sequences are referred as Low Discrepancy Sequences (LDS) since the points are more evenly distributed $[0, 1]^d$. Here, discrepancy is the measure of uniformity of the sequence. For Monte Carlo method, the convergence is of the order $O(N^{-1/2})$ compared to $O(\log^d(N)/N)$ for QMC because of the Koksma-Hlawka inequality (Goncu, 2009). Quasi-random sequences have different variants such as Halton, Scrambled (randomized) Halton and Hammersley sequences. The Halton sequence construction, defined via the radical inverse function, uses coprime numbers as their bases (Halton, 1964). In the Halton sequences, the lack of correlation between the radical inverse functions of different bases can lead to inadequate distribution of two-dimensional projections. The scrambled Halton sequence corrects this defect by redistributing the projections more accurately. Halton and Scrambled Halton sequences have advantages over other sequences in terms of extension of the domain's dimensionality (Chunduri *et al*, 2018).

Here, we use Scrambled Halton LDS for a parameter sweep as in Chunduri *et al*. (2018). However, we extend the application to the multiscale model by applying the algorithm

interchangeably for the pedestrian and infection models. The results are then compared to lattice sweep to show the efficiency of LDS in terms of faster convergence and execution time. We study the problem of infection spread in a pedestrian winding queue using this approach.

2.5. Application to Pedestrian Queue

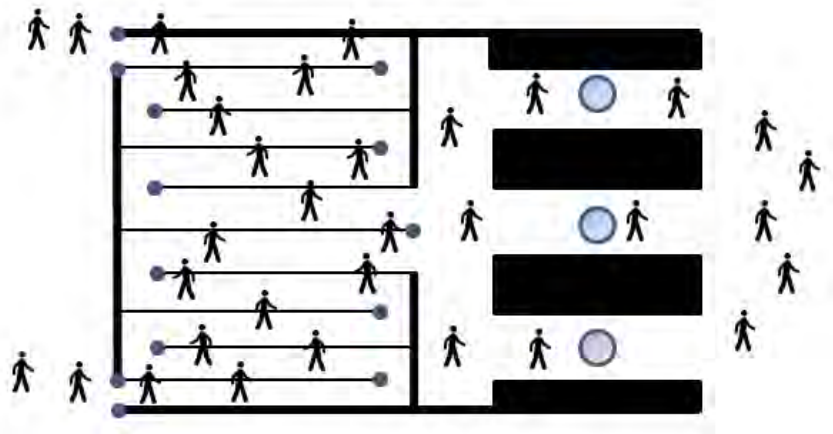

(a)

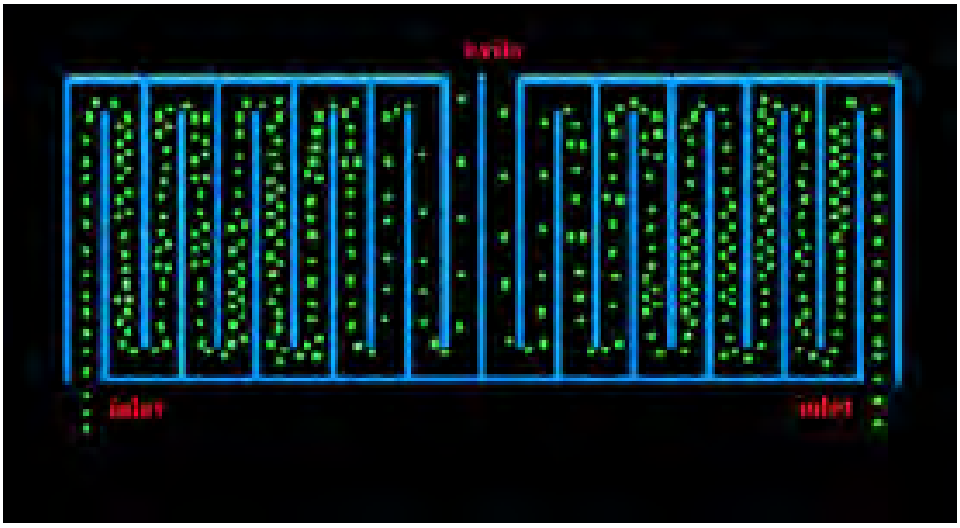

(b)

Figure 3. (a) Schematic layout of security check region (b) Evolution of pedestrians (t=125s) from simulation of a pedestrian queue in a rectangular layout.

Pedestrian winding queues are an unavoidable component of crowd management in places like airport security checks, religious and entertainment venues. In Derjany *et al*. (2020), different queue configurations are evaluated in terms of contact generation and infection propagation among neighboring pedestrians. One such pedestrian queue configuration is shown in Figure 3 as an example. The modeling work-flow shown in Figure 4, consists of applying the parameter sweep to the pedestrian parameters first. The resulting trajectories are input to the infection model, incorporating a parameter sweep of infection variables.

Table 1 lists the ranges of the pedestrian and infection parameters considered in the parameter sweep study. Both lattice and LDS parameter sweeps are used with these ranges to examine their efficiency in reducing the number of simulations needed to adequately cover the design space.

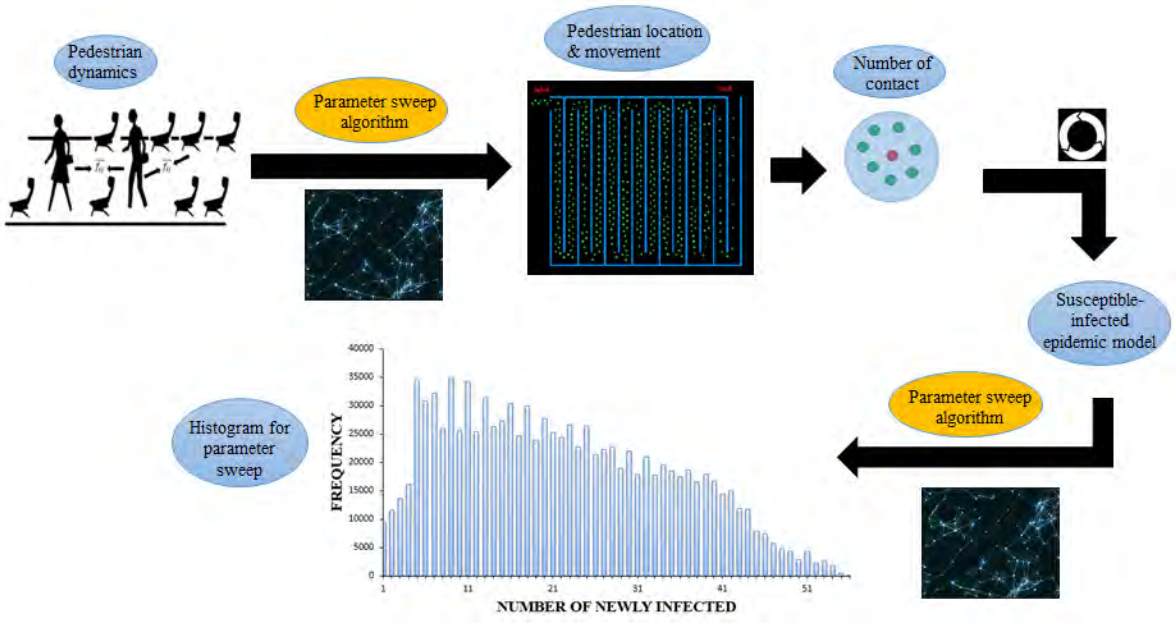

Figure 4. Schematic depiction of the multi-scale approach.

Table 1. Parameters range of the pedestrian-infection model formulation.

Parameter	V_0	δ_1	δ_2	R	P_{inf}
Range	3.2-5.4 ft/s	15-25 in	25-40 in	36-84 in	0.025-0.225
Selected increments	0.1-0.2	1-5	1-5	0.5-12	0.01-0.025

For both Lattice and LDS sweeping algorithms, a coarse grid is first considered, and then refined until convergence is attained. At each grid size, a histogram with the targeted variable (the number of newly infected pedestrians) versus the frequency of occurrence is plotted. Four descriptive moments of the probability distribution, mean, standard deviation, skewness and kurtosis are analyzed to determine convergence. Once the relative difference of the output between two grid sizes is lower than a predetermined tolerance as shown in equation (8), further refinement of the parameter space is not required.

$$\frac{V_i - V_{i+1}}{\left[\frac{V_i + V_{i+1}}{2}\right]} \leq \varepsilon \tag{8}$$

Here V is a statistical moment and ε is a tolerance value. The selection of the tolerance order depends on the statistical moment. For instance, for the relative mean, ε is of the order of 10^{-3} compared to 10^{-1} for the root of standard deviation, skewness and kurtosis. The abrupt drop of the relative kurtosis from a value greater than unity to a value of order 10^{-1} indicates that the histogram distribution is invariant between the runs. When these conditions are met, convergence is attained.

3. RESULTS & DISCUSSION

3.1 Infection dynamics at the Airport Security Check

We first present the multiphysics model results in this section. This is followed by results on the algorithmic developments in reducing the parameter variations needed to cover the space efficiently. Reports indicate that travelers are delayed for more than an hour at screening checkpoints, causing significant economic burden on airlines (Bender 2016). Screening procedure at checkpoints only involves the passengers and their carry-on baggage. However, no equipment is available for use to detect viral contagions during an outbreak. Consequently, security checkpoints with people congregated in winding queues are a potential hotspot for infectious disease spread.

We utilized cell phone location data for Orlando International Airport (MCO) averaged over a week during the October 2017 flu season to statically estimate the inputs to the pedestrian dynamics model in terms of, key locations, pedestrian numbers and densities. This is expected to change due to the effect of COVID on air travel in recent months, however, these results serve as a demonstration of the approach and can be updated with more relevant data. In Figure 5, we show the bubble maps of the data and indicate that travelers are concentrated near the security check points for terminals A and B in the morning rush hour. An aggregate of such maps at different times is used to evaluate how crowd sizes vary and to generate inputs to the pedestrian dynamics. These are then used to model the pedestrian movement though the security area and the effect of different layout configurations. Eight configurations in square and rectangular shapes are used to study the effect of layout shape. Further, the impact of using walls as opposed to rope stanchions for directing the queue, as well as the effect of forcing a

single file queue are evaluated for effectiveness as mitigation strategies. We identify specific layouts that more effective than currently used ones, however the effect of layout shape is reduced when the contact distance is higher (e.g. 2 m in aerosol transmitted diseases). We find that walls and single file queue or a combination of both reduces the number of contacts significantly.

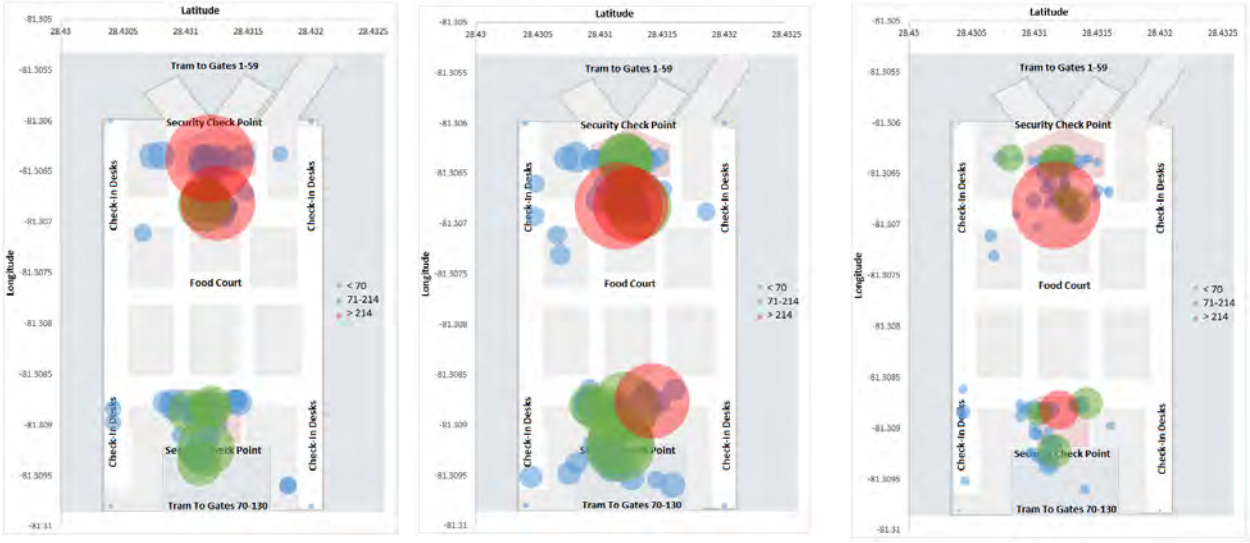

Figure 5. Bubble maps of the location of passengers in the morning, afternoon and evening hours used as input for pedestrian dynamics simulations

In investigating the relation between the layout shape and the contact among pedestrians in queues, we simulate different security line winding queues by changing the aisles and zones layout based on actually observed queue configurations in airports (Figure 6). With time evolution, the pedestrians move forward in the sequence to reach the exit. It is expected that the aisle's length, direction and structure within the control area, and the distribution of turn corners have an effect on the contact between pedestrians.

We consider the case of pedestrians arranging in a rectangular queue. At initial conditions, the pedestrians are distributed in abreast (side-by-side) manner in the aisles. The formation of groups (family members, group of tourists, etc.) is taken into consideration by the close abreast queues whereas individual travelers tend to form a more spaced single line as mentioned in the formulation section.

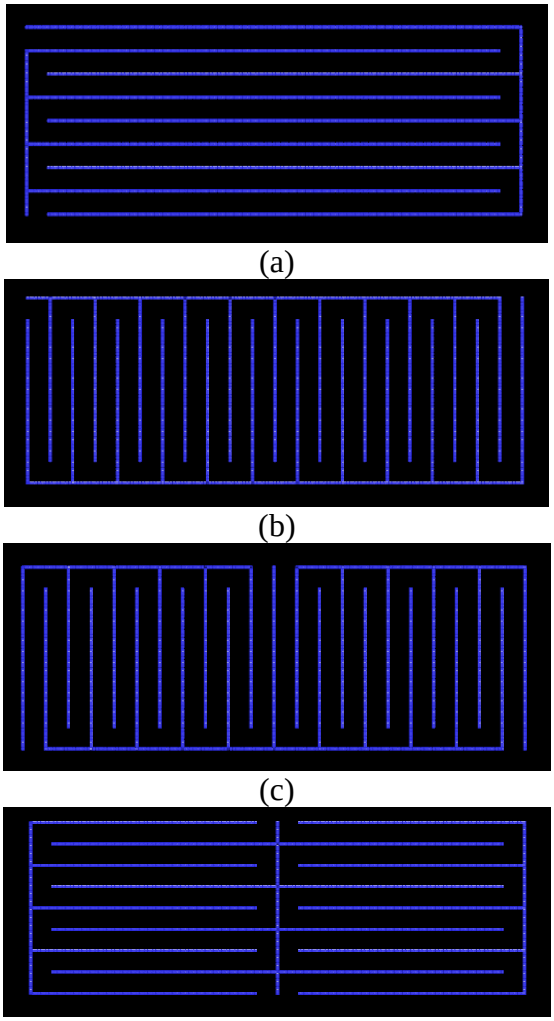

Figure 6. Rectangular winding queue layouts: (a) Config.1, (b) Config.2, (c) Config.3, (d) Config.4.

Four different rectangular queue configurations of the same area, as shown in Figure 6, are analyzed. The four rectangular floor plans are either split vertically (configurations (b) and (c)) or horizontally (configurations (a) and (d)). Configurations (a) and (b) have one inlet and one exit whereas configurations (c) and (d) have two inlets and two exits due to the existence of separated zones. The width of the pedestrian lanes remains 1 meter, which allows some pedestrians belonging to the same group to form a double line.

Instead of limiting the analysis to certain disease type or mechanism, we generalize the study by sweeping the infection parameters (infection probability and contact radius) over their ranges of definition. We vary the contact distance between 2.1 m and 0.9 m which are representative of aerosol and coarse droplet mechanisms respectively. Similarly, the infection probability (P_{inf}) is varied as a parameter up to a value of 0.2 to represent various levels of infectivity.

The mean number of newly infected pedestrians is then obtained by combining the number of contacts within a given contact radius, with the infection transmission probability described earlier. The mean number of newly infected is binomially distributed to account for the demographic stochasticity in the immunity and receptivity of the susceptible population. Under different infection scenarios, the mean number of newly infected exposed individuals is obtained. In the following, only the peak dispersion of the disease (the mean of the binomial distribution) among the susceptible population is plotted over the parameters space of variation.

With the commonly used rope separators and at a proximate, direct contact via coarse droplets (radius of infection less than 1.2m), the infective has influence on only the directly

adjacent aisles on both sides. However, infection also relies on the transmission probability. In other words, not every contact will lead to infection. For a defenseless (unimmunized) individual, the probability to contract the disease alters between 2.5 and 20% depending on the disease development time and its survival in the ambient environment. Combining the contact data with the infection model leads to the mean distribution of infection over the probability range. Configurations 3 is the best layout for all transmission probabilities, followed by configuration 2 (Figure 7). In configuration 2, the vertical aisles are short, which means less capacity of pedestrians. Configuration 3 has the same aisle geometry as of configuration 2. However, the pedestrian will exit the queue earlier (half way) compared to that of configuration 2 which results in lower exposure time. Configurations 1 and 4 result in a higher mean number of infections. These configurations have long open aisles compared to configurations 2 and 3 with the lower aisle length. Therefore, more pedestrians are involved and interaction occurs more frequently with pedestrians from neighboring aisles in these two configurations. Configuration 1 is the least favorable layout because diverse pedestrians from both sides come into proximity more frequently than in configuration 4 with comparatively shorter aisles. Configuration 4 is worse than configuration 2 because at the common corners between the left and right zones, the infective comes into contact with additional pedestrians from the neighboring zones.

Figure 10 also shows the results of repeating the transmission probability variation over the same range, but assuming aerosol transmission mechanism with a longer contact radius of 2.1 m. Configuration 3 still results in the lowest number of contacts for both rope and wall separators. For rope separator, we observe the same pattern of results as with the coarse

droplets transmission mechanism, but with increased infection spread. The similarity between the configurations increases especially at low transmission probabilities. Therefore, the results of configurations 2 and 3, as well as configurations 1 and 4 overlap. At 2.1 m radius, the dispersion of the fine viral particles crosses the aisle boundaries to two adjacent aisles on each side. Here, the findings of configurations 2 and 3 are nearly identical since the aisles are distributed in the same manner except that configuration 3 has two separated zones. When the transmission radius expands to many neighbouring aisles, pedestrians of one zone in configuration 3 come into contact not only with other pedestrians within the same zone, but to others in the adjacent zone. Accordingly, configurations 2 and 3 have the same behavior. Here, the separation of these two groups has no effective role in reducing contact. The same principle applies to configurations 1 and 4; the offset between the data of configurations 1 and 4 is reduced compared to that of coarse droplet transmission mechanism for the same reason. Configuration 1 remains the worst layout, especially at higher probabilities, due to the elongated, abundant contact between pedestrians from adjacent aisles.

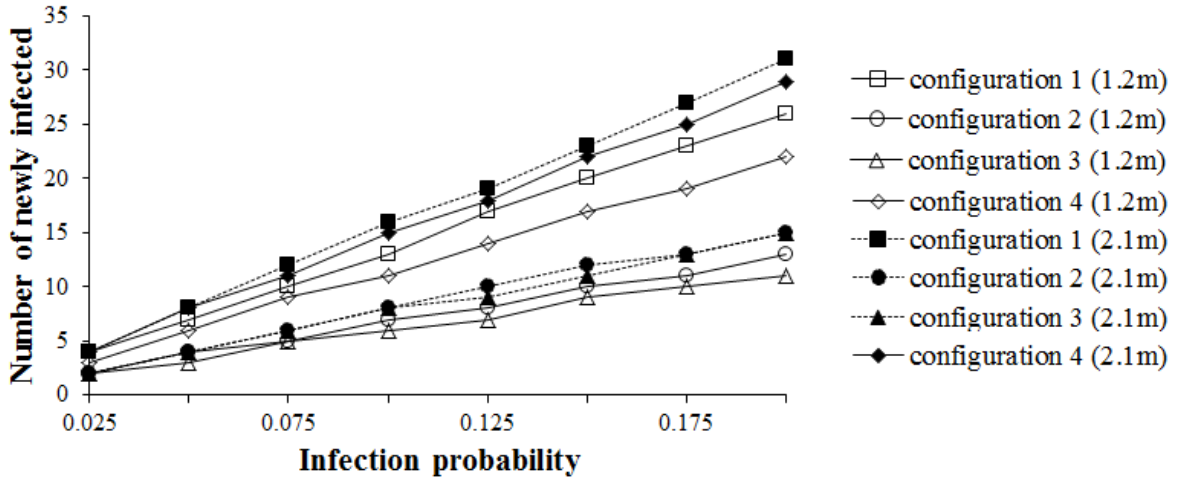

Figure 7. Infection distribution profile for different abreast queue configurations at contact radii of 1.2m (coarse droplets) and 2.1m (fine aerosols).

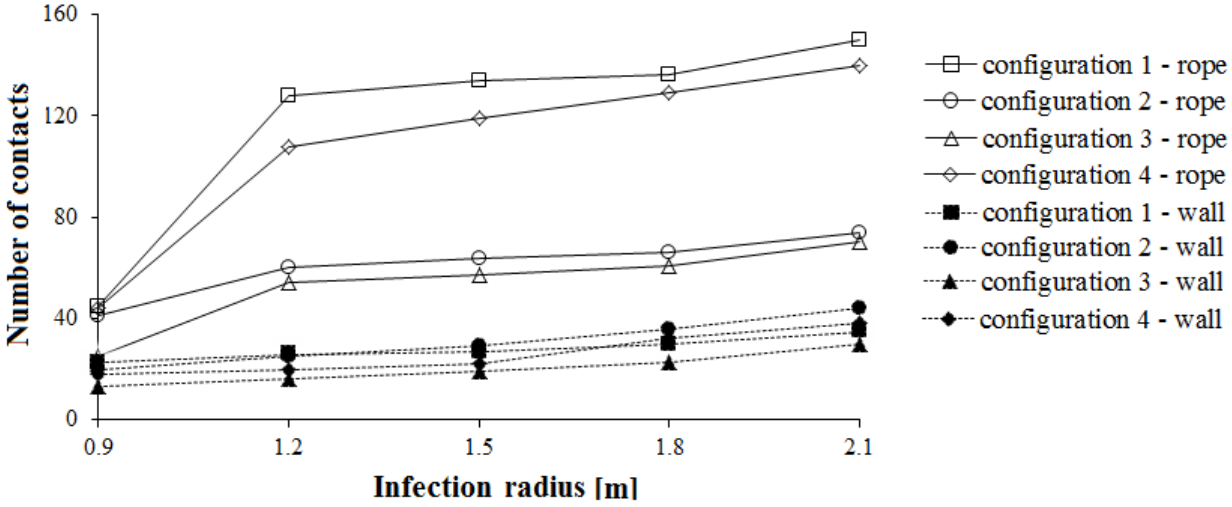

Figure 8. Contact distribution for different abreast queue configurations. The contact radius is varied for both wall and rope aisle separation scenarios

We now explore the contacts generated between pedestrians in the four configurations assuming different infection mechanisms represented by the radius variation. We suggest placing temporary walls between the aisles to suppress the propagation of the outbreak among the waiting crowd. For rope separators previously evaluated, contact extends to pedestrians in

the neighboring aisles, whereas for temporary walls, transmission due to contact is limited only between the pedestrians within the same aisle.

Configurations 2 and 3 result in lower number of infections for rope separators, across the range of infection radii from 0.9 to 2.1 m as shown in Figure J. As explained, for aisles separated with ropes, shorter aisles lead to lower exposure of an infective resulting in this behavior. For walls, the combination of the radius of infection, as well as the interaction time within the aisles and at the corners alter the results (Figure 8). Each combination of contact radius and queue layout generates a different number of newly infected individuals. At low radii, short-aisle and low exit time configurations are favorable. At higher radii, configurations with less turning corners are better. The wall separator has drastically reduced the number of infections compared to the conventionally used rope stanchions.

These results indicate how the pedestrian movement layouts and strategies affect the infectious disease spread. They also point out the need for large scale parameter sweeps to address the entire design space. In the following section we discuss the application of the novel parameter sweep algorithms to this problem.

3.2 Application of Parameter Sweep Algorithms

The workflow in figure 4 is applied with parametric variations in Table 1 as follows. First a 5D lattice parameter sweep is performed by varying the three pedestrian dynamics parameters, and two infection model parameters over an evenly spaced lattice grid. This baseline is compared with two other situations in which, 2D lattice grid for infection model is combined with 3D LDS for pedestrian dynamics parameters, and 3D Lattice grid for pedestrian

dynamics is combined with 2D LDS parameter sweep for the infection model. The convergence and model implications in each case are discussed.

3.2.1 Lattice Parameter Sweep

The lattice-based parameter sweep is applied to the parameters of the two models separately. The trajectories are obtained from the pedestrian model by varying pedestrian maximum speed ($v_A + v_B$) and allowable proximate pedestrian-pedestrian distances (δ_1 and δ_2). The resulting contact data (m_i) for each simulation is used in the infection model by varying the contact radii (R) and transmission probability (P_{inf}). Changing the increment sizes for these five parameters on a lattice grid results in six parameter sweeps with 6480, 11664, 144900, 2125000, 4165392 and 8245776 numbers of simulations.

Each of these simulations generates an average number of infections. For example, consider a case where the infective has an infectious disease (e.g. COVID-19) which is at a stage where the transmission probability is 0.1 and the infection radius is 72 in. Consider that this infective passes through the pedestrian queue shown in figure 1. If the pedestrians in the queue have an average unobstructed speed of 4 ft/s and maintain a distance of 3 ft between each other, this results in an average of 8 new infections. The average here implies that the position of the infective in the queue is not known *aprioiri* and this is varied and averaged to obtain the number of new infections. This result is one specific output for these specific input parameter values. Figure 9 shows this output as a function of frequency for the parameters varied on different lattice grids.

There is uncertainty with respect to both pedestrian parameters like speed and distance between people, and also infection parameters like transmission probability and infection

spread radius. By varying all of these parameters we can get a comprehensive idea of how disease would spread. If these parameters are varied on a coarse grid like in Figure 3 (a), some of the variations are not captured. As the parameter lattice is refined more of these variations are captured. A similar parameter sweep with an intervention would show how the infection spread would change across the entire parameter space.

Note that convergence can be visually ascertained when the shape of the histogram remains proportionally the same while increasing the number of simulations. In this case, convergence starts from Grid 4 in Figure 9(d). The convergence is also validated theoretically by using statistical variables mentioned earlier.

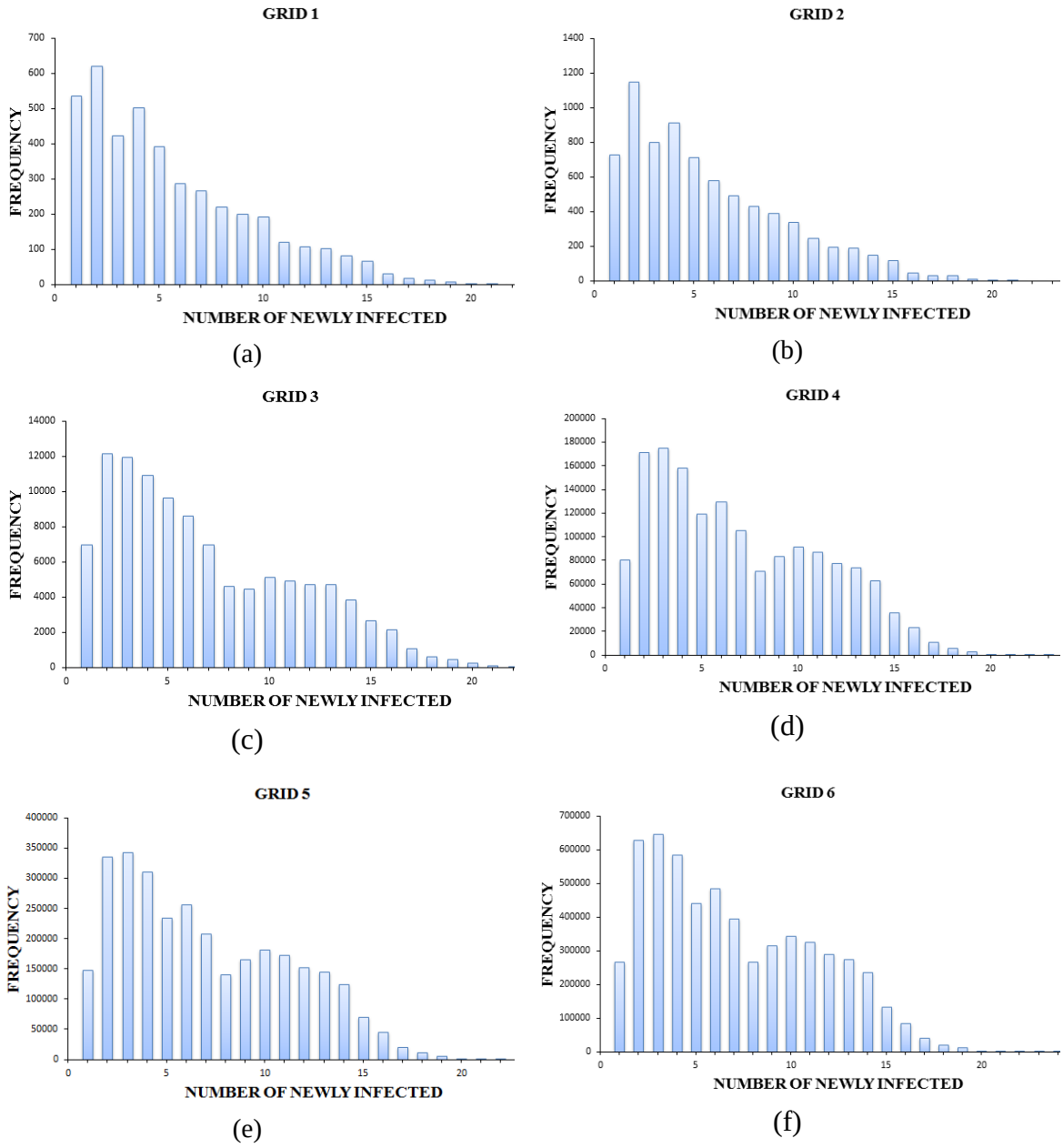

Figure 9. Infection distribution histograms for (a) 6480, (b) 11,664, (c) 144,900, (d) 2,125,000, (e) 4,165,392 and (f) 8,245,776 grid points using 5D Lattice method.

3.2.2 Mixed LDS and Lattice Parameter Sweep

Here, LDS based parameter sweep is applied to the pedestrian dynamcis component of the multiscale model, i.e. to the three pedestrain dynamics parameters in Table 1, while the two infection model parameters are varied on a lattice grid. Six parameter grids with successively finer spacing are considered. For Grids 1 and 2 the infection lattice parameter spacing corresponding to Grid 2 of the 5D lattice sweep shown in Figure 9 (b) is used. For Grids 3-6 a finer lattice spacing corresponding to Grid 4 of the 5D lattice sweep shown in Figure 9 (d) is used. The LDS algorithm is used to generate sequences for the 3D pedestrian dynamics parameter space. This combination of parameters leads to six sequences with 4050, 11250, 157500, 525000 and 787500 simulations respectively. Figure 10 shows the histograms of the combined lattice and LDS approach. With a low number of combinations for the speed and distance parameters and a coarse lattice grid for the infection parameters, the histograms corresponding to Grids 1 and 2 do not capture the distribution of the newly infected at high numbers. Grids 3-6 can capture the distribution of infections much more effectively as shown in Figure 10. It can be noted that the convergence is reached by 157,500 simulations in this case compared to the 2,125,000 simulations needed with 5D lattice parameter sweep.

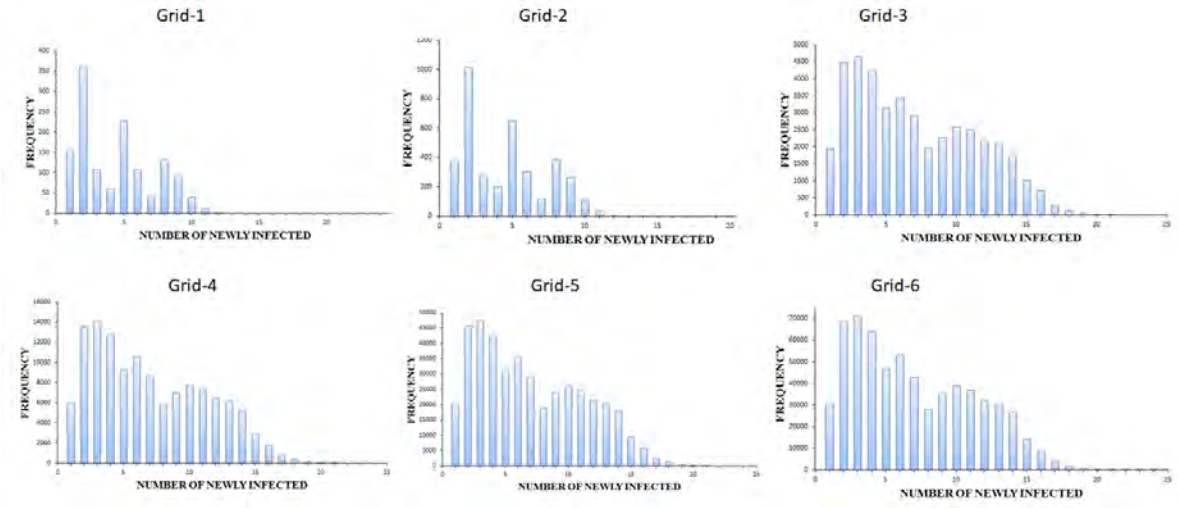

Figure 10. Infection distribution histograms for (a) 4,050, (b) 11,250, (c) 52,500, (d) 157,500, (e) 525,000 and (f) 787,500 grid points using 3D pedestrian LDS combined with 2D Lattice method.

A similar analysis is conducted with 2D LDS parameter sweep for the infection parameters, combined with a 3D lattice sweep for pedestrian dynamics parameters. The variation of parameters again results in six simulation grid sizes with 108000, 144000, 288000, 809600, 1012000 and 1214400 simulation sequences. We find that the visual and numerical convergence in this case happens for Grid-4 with 809600 simulations (see Figure 11).

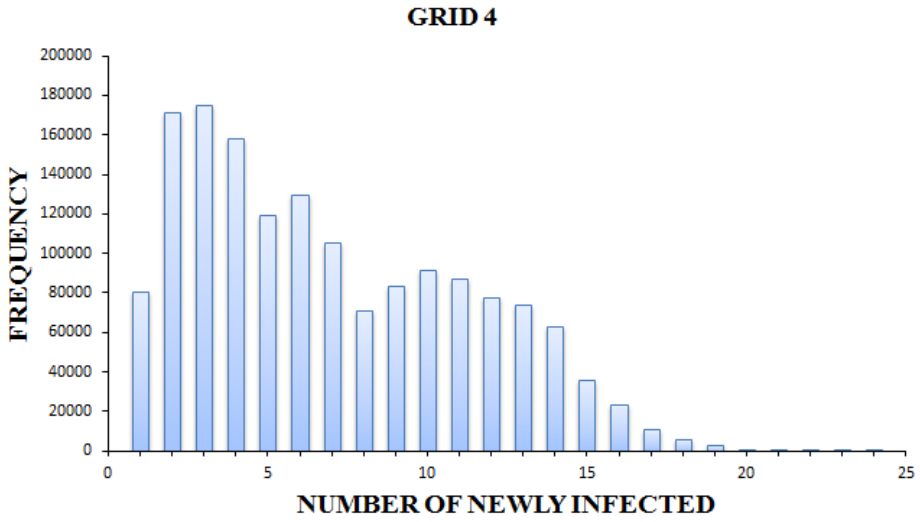

Figure 11. Infection distribution histogram for 809,600 grid points (convergence) using 3D pedestrian Lattice combined with 2D LDS

3.2.3 Analysis of Convergence Measures

Figure 12 shows the convergence metrics for the three parameter sweeps conducted in this work. The convergence is analyzed by comparing the four statistical measures mean, standard deviation, kurtosis and skewness. In the case of the 5D lattice parameter sweep, convergence is attained at Grid 4 with 2,125,000 simulations. The relative difference of the mean, standard deviation, skewness and kurtosis values are within tolerance when a finer lattice grid with more simulations is used.

The values of the relative mean and standard deviation vary minimally as the number of simulations is increased, whereas the skewness and kurtosis increase with parameter refinement, which indicates the biasing of the histograms toward a high-frequency value of 3 newly infected pedestrians. The distribution of the histogram in bell shape (Figure 10) around the peak accounts for the stochasticity of the model. The histogram's peak is attained at 3 newly infected members, which indicates that there is a highest probability of one infective

generating 3 new infections for the pedestrian queue studied here. However, in preventive planning one should account for the worst-case scenario. The plot extends to a worst case scenario of 24 possible infection cases with a mean of about 7 new infections.

In the case of 2D LDS –3D Lattice parameter sweep the same mean of 6.98 with a close standard deviation is obtained at Grid-4 with only 809,600 simulations compared to 2,125,000 required for 5D Lattice sweep. The convergence is reached with the same increments used previously for the pedestrian model parameters and only 200 low discrepancy sequences to cover the 2-Dimensional infection parameters space. The computational effort is less than 50% compared to that required for a 5D lattice. The plot in Figure 12 showing the relative difference of the four statistical moments behaves in a similar manner as that of 5D lattice after convergence is reached. When LDS parameter sweep is applied for the three parameters in the pedestrian movement model convergence is attained at 157,500 simulations with a similar mean of 7.04. Again, at Grid 4, the relative differences of the statistical moments converge toward a zero value as shown in Figure 6. The parameters increments at convergence for the three parameter sweeps are shown in Table 2.

Table 2. Parameters increments at convergence

Parameters increments at convergence	5D Lattice	3D Lattice-2D LDS	3D LDS-2D Lattice
$v_A + v_B$	0.1	0.1	300 sequences
δ_1	1	1	
δ_2	1	1	
R	2	200 sequences	2
P_{inf}	0.01		0.01

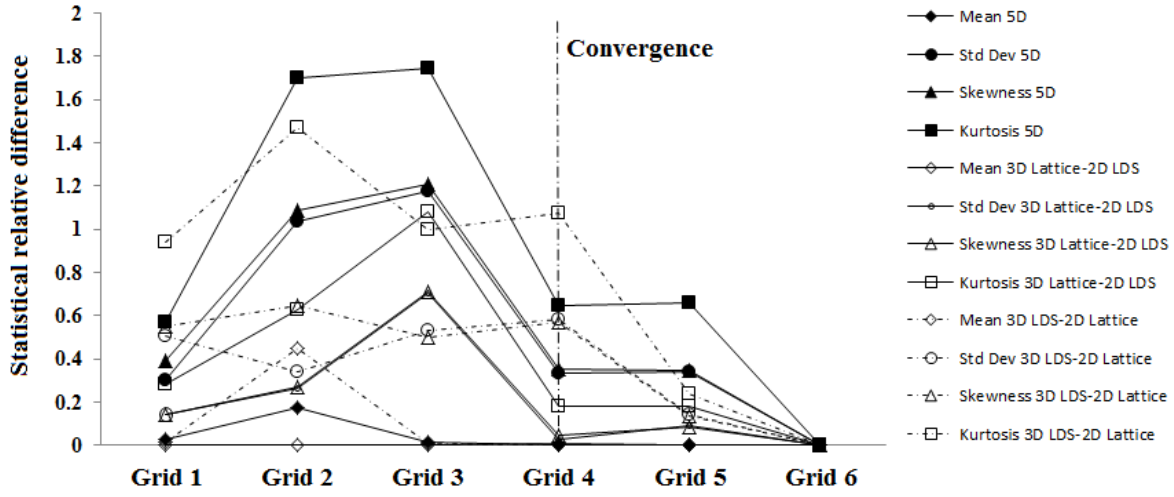

Figure 12. Statistical moments distribution with increment refinement for the three parameter sweep methods.

3.3 Discussion

A multiphysics model combining social-force-based pedestrian dynamics and the individual based stochastic infection dynamics model has been formulated. The model is used to study the dynamics of infectious disease spread in airplanes and airports. Specific air-travel-related policies that potentially mitigate diseases spread are identified. We find that the layout of winding queues in airport security check influences the number of new infections. Policies like using wall separators for crowd control are effective in reducing infectious disease spread. The modeling approach developed here is generic and can be readily modified to other directly transmitted infectious diseases and dense pedestrian spaces, however, the problem is computationally intensive as it requires large parameter sweeps. Here we have demonstrated application of new algorithms based on low discrepancy sequences for increasing the efficiency of the parameter sweep

Low Discrepancy Sequences have found various applications in various fields. For instance, multi-dimensional integrals are often evaluated using quasi-stochastic Monte Carlo method (Cools, 2002). Parameter sweep for high dimensional space is a closely related problem. A disadvantage with pseudo-random finite sequences is that they are not equidistributed over the domain of integration which can yield asymptotically worse convergence rate. The usage of increased equidistributed random sequences improves accuracy, but can be computationally expensive (Sen, 2006). The lattice-based space repartition is a uniform distribution method that partitions the domain uniformly. This method has a much higher computational cost compared to the pseudo-random sequences. Low discrepancy sequences using quasi-random numbers were originally introduced to improve convergence in comparison to Monte Carlo integration, but they can also address the high computation time problem for large parameter sweeps on parallel clusters. Low-discrepancy (quasi-random) sequences have an advantage of being more equidistributed than pseudo-random numbers and are more efficient both with respect to space coverage and convergence. Chunduri et al (2018) used the Low Discrepancy Sequence based parameter sweep for analyzing pedestrian movement in an airplane boarding and show that this approach significantly reduces the number of simulations needed to adequately cover the parameter space. Many engineering and public health problems are multidisciplinary and multiscale in nature. For example, consider the infectious disease spread in a pedestrian queue considered in this study. The contact analysis is based on pedestrian movement and mixing at one scale, while the infectious disease propagation is at another scale. The results of this study show that there is a significant reduction in computational requirements compared to lattice based

parameter sweep, when the LDS method is used in one of the sub-models. There is an order of magnitude improvement in the number of simulations needed to adequately cover the parameter space as shown in Figure 13. Another significant advantage of LDS approach is that if further refinement of the parameter space is needed, the scrambled Halton sequence adds to the existing sequence, enabling reuse of the existing simulations. This facilitates the restart of parameter sweep problems.

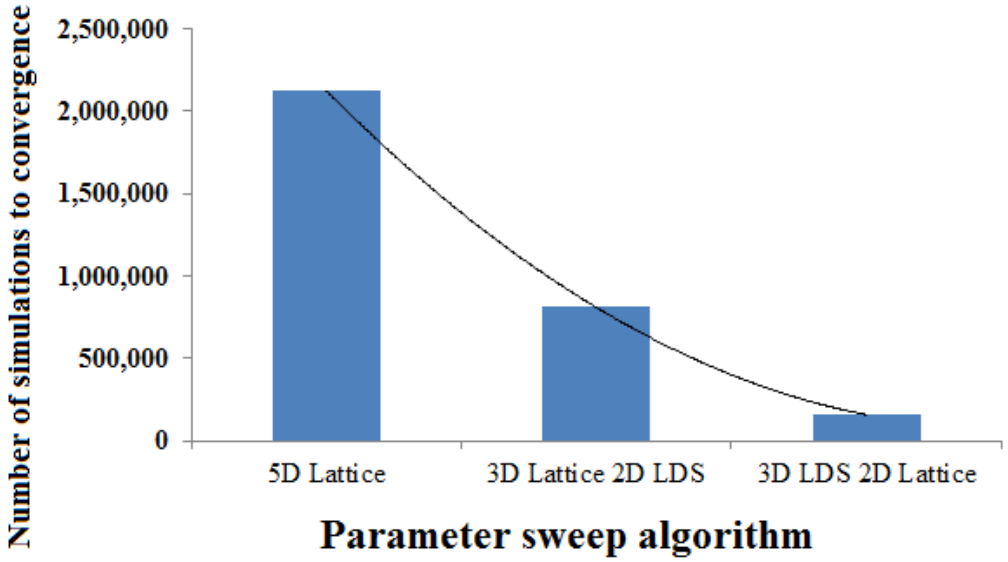

Figure 13. Number of simulations required for each parameter sweep algorithm.

4. CONCLUSIONS

In this report, we model the infectious disease spread in a pedestrian winding queue and analyze the parameter space using novel parameter sweep. A multiscale model is formulated combining social force based pedestrian dynamics model with an individual stochastic epidemiological model. The model is applicable to many directly transmitted diseases including COVID-19 based on the input parameters. A five dimensional space

consisting of three pedestrian dynamics parameters (free speed, cut-off distances) and two epidemic model parameters (transmission probability and infection radius) are considered for the parameter sweeps.

A uniform Lattice-based parameter sweep is first used to analyze the five dimensional parameter space. In each dimension, the increment is taken to be constant, generating a uniformly distributed vector of values within the range of definitions of each parameter. A coarse uniform partition of the parameters vectors may leave out some critical parameter combinations, which can lead to deficiencies in the results. This is undesirable for assessing preventive strategies that inhibit the disease outbreak. A fine uniform lattice is computationally expensive both for covering the parameter space and convergence checks. We find that 2,125,000 simulations are needed to obtain convergence using the lattice approach.

An effective alternative to lattice parameter sweep is a Scrambled Halton Low Discrepancy Sequence approach. In the multidisciplinary model used here, we find that use of LDS in even one of the interconnected models is effective in reducing the required number of simulations. When LDS is used to generate sequence for three dimensional parameter space for the pedestrian model and the conventional lattice is used for the infection model, the convergence is achieved with 157 500 simulations, which is an order of magnitude improvement in computational efficiency. When LDS is used for the two dimensional parameter space of the infection model, the parameter space can be covered using 809,600 simulations.

A mean of 7 newly infected individuals is obtained for the distribution of new infections over the entire parameter space. The number of infections may extend up to 24 cases with the

highest probability obtained for 3 cases. Given the stochasticity and uncertainty in infection spread and human behavior. Interventions to reduce infections need to be effective across many scenarios. The modeling and parameter sweep approach developed in this study can help identify such interventions.

REFERENCES

1. Heesterbeek, H., Anderson, R.M., Andreasen, V., Bansal, S., De Angelis, D., Dye, C., Eames, K.T., Edmunds, W.J., Frost, S.D., Funk, S. and Hollingsworth, T.D. (2015). Modeling infectious disease dynamics in the complex landscape of global health. Science, 347(6227)
2. Merler, S., Ajelli, M., Fumanelli, L., Gomes, M., Piontti, A., Rossi, L., Chao, D., Longini, I., Halloran, M. and Vespignani, A. (2015). Spatiotemporal spread of the 2014 outbreak of Ebola virus disease in Liberia and the effectiveness of non-pharmaceutical interventions: a computational modelling analysis. The Lancet Infectious Diseases, 15(2), 204-211.
3. Namilae, S., Srinivasan, A., Mubayi, A., Scotch, M. and Pahle, R. (2017). Self-propelled pedestrian dynamics model: Application to passenger movement and infection propagation in airplanes. Physica A: Statistical Mechanics and its Applications, 465, 248-260.
4. Barrat, A., Cattuto, C., Tozzi, A. E., Vanhems, P., & Voirin, N. (2014). Measuring contact patterns with wearable sensors: methods, data characteristics and applications to data-driven simulations of infectious diseases. Clinical Microbiology and Infection, 20(1), 10-16.

5. Smieszek, T., Fiebig, L., & Scholz, R. W. (2009). Models of epidemics: when contact repetition and clustering should be included. Theoretical biology and medical modelling, 6(1), 1-15.
6. De Cao, E., Zagheni, E., Manfredi, P., & Melegaro, A. (2014). The relative importance of frequency of contacts and duration of exposure for the spread of directly transmitted infections. Biostatistics, 15(3), 470-483.
7. Cai, J., Sun, W., Huang, J., Gamber, M., Wu, J., & He, G. (2020). Indirect virus transmission in cluster of COVID-19 cases, Wenzhou, China, 2020. Emerging infectious diseases, 26(6), 1343.
8. Coronavirus: 5 More Cases at Osaka Concert Venues, https://www.nippon.com/en/news/ntv20200306001/coronavirus-5-more-cases-at-osaka-concert-venues.html
9. Coronavirus toll mounts at Seattle-area nursing home, https://www.latimes.com/world-nation/story/2020-03-09/la-na-nursing-home-positive-coronavirus-tests
10. Mizumoto, K., & Chowell, G. (2020). Transmission potential of the novel coronavirus (COVID-19) onboard the diamond Princess Cruises Ship, 2020. Infectious Disease Modelling, 5, 264-270.
11. Why a South Korean Church Was the Perfect Petri Dish for Coronavirus, https://www.wsj.com/articles/why-a-south-korean-church-was-the-perfect-petri-dish-for-coronavirus-11583082110

12. Xu, X. W., Wu, X. X., Jiang, X. G., Xu, K. J., Ying, L. J., Ma, C. L., & Sheng, J. F (2020). Clinical findings in a group of patients infected with the 2019 novel coronavirus (SARS-Cov-2) outside of Wuhan, China: retrospective case series. bmj, 368.
13. Burstedde, C., Klauck, K., Schadschneider, A., & Zittartz, J. (2001). Simulation of pedestrian dynamics using a two-dimensional cellular automaton. Physica A: Statistical Mechanics and its Applications, 295(3-4), 507-525.
14. Henderson, L. F. (1971). The statistics of crowd fluids. nature, 229(5284), 381-383.
15. Okazaki, S., & Matsushita, S. (1993). A study of simulation model for pedestrian movement with evacuation and queuing. In International Conference on Engineering for Crowd Safety (Vol. 271).
16. Helbing, D., & Molnar, P. (1995). Social force model for pedestrian dynamics. Physical review E, 51(5), 4282.
17. Helbing, D., Farkas, I., & Vicsek, T. (2000). Simulating dynamical features of escape panic. Nature, 407(6803), 487-490.
18. Helbing, D., Hennecke, A., & Treiber, M. (1999). Phase diagram of traffic states in the presence of inhomogeneities. Physical Review Letters, 82(21), 4360.
19. Wei-Guo, S., Yan-Fei, Y., Bing-Hong, W., & Wei-Cheng, F. (2006). Evacuation behaviors at exit in CA model with force essentials: A comparison with social force model. Physica A: Statistical Mechanics and its Applications, 371(2), 658-666.

20. Helbing, D., Farkas, I. J., Molnar, P., & Vicsek, T. (2002). Simulation of pedestrian crowds in normal and evacuation situations. Pedestrian and evacuation dynamics, 21(2), 21-58.
21. Li, Z., & Jiang, Y. (2014). Friction based social force model for social foraging of sheep flock. Ecological modelling, 273, 55-62.
22. Mehran, R., Oyama, A., & Shah, M. (2009, June). Abnormal crowd behavior detection using social force model. In 2009 IEEE Conference on Computer Vision and Pattern Recognition (pp. 935-942). IEEE.
23. Zanlungo, F., Ikeda, T., & Kanda, T. (2011). Social force model with explicit collision prediction. Europhysics Letters, 93(6), 68005.
24. Lämmel, G., & Plaue, M. (2014). Getting out of the way: Collision-avoiding pedestrian models compared to the realworld. In Pedestrian and Evacuation Dynamics 2012 (pp. 1275-1289). Springer, Cham.
25. Namilae, S., Derjany, P., Mubayi, A., Scotch, M., & Srinivasan, A. (2017). Multiscale model for pedestrian and infection dynamics during air travel. Physical review E, 95(5), 052320.
26. Derjany, P., Namilae, S., Liu, D., & Srinivasan, A. (2020). Multiscale model for the optimal design of pedestrian queues to mitigate infectious disease spread. PLoS one, 15(7), e0235891.
27. Youn, C., & Kaiser, T. (2010). Management of a parameter sweep for scientific applications on cluster environments. Concurrency and Computation: Practice and Experience, 22(18), 2381-2400.

28. Nelson, W. R., Hirayama, H., & Rogers, D. W. (1985). EGS4 code system (No. SLAC-265). Stanford Linear Accelerator Center, Menlo Park, CA (USA).
29. Basney, J., Livny, M., & Mazzanti, P. (2000). Harnessing the capacity of computational grids for high energy physics. In Conference on Computing in High Energy and Nuclear Physics (pp. 610-613).
30. Osterholm M. T et al., (2015), Transmission of Ebola viruses: what we know and what we do not know, MBio, 6(2), p. e00137-15.
31. Judson, S., Prescott, J., & Munster, V. (2015). Understanding ebola virus transmission. Viruses, 7(2), 511–521.
32. Nikiforuk, M., Cutts, T. A., Theriault, S. S., & Cook, B. W. (2017). Challenge of liquid stressed protective materials and environmental persistence of ebola virus. Scientific reports, 7(1), p. 4388.
33. Clark, R. P., & de Calcina-Goff, M. L. (2009). Some aspects of the airborne transmission of infection. Journal of the Royal Society Interface, 6(suppl_6, pp. S767–S782.
34. Li, R. W. K., Leung, K. W. C., Sun, F. C. S., & Samaranayake, L. P. (2004). Severe Acute Respiratory Syndrome (SARS) and the GDP. Part I: Epidemiology, virology, pathology and general health issues. British dental journal, 197(2), p. 77.
35. Yuen, K. Y., & Wong, S. S. Y. (2005). Human infection by avian influenza A H5N1. Hong Kong Medical Journal.

36. Bourouiba, L., Dehandschoewercker, E., & Bush, J. W. (2014). Violent expiratory events: on coughing and sneezing. Journal of Fluid Mechanics, 745, pp. 537–563.
37. Gupta, J. K., Lin, C. H., & Chen, Q. (2009). Flow dynamics and characterization of a cough. Indoor air, 19(6), pp. 517–525.
38. Mangili, & Gendreau, M. A. (2005). Transmission of infectious diseases during commercial air travel. The Lancet, 365(9463), pp. 989–996.
39. Centers for Disease Control and Prevention (2021, May). *Scientific Brief: SARS-CoV-2 Transmission.* COVID-19, https://www.cdc.gov/coronavirus/2019-ncov/science/science-briefs/sars-cov-2-transmission.html
40. Friesema H. M et al., (2009). Norovirus outbreaks in nursing homes: the evaluation of infection control measures. Epidemiology & Infection, 137(12), pp. 1722–1733.
41. Jaax, N et al., (1995). Transmission of Ebola virus (Zaire strain) to uninfected control monkeys in a biocontainment laboratory. The Lancet, 346(8991–8992), pp. 1669–1671.
42. Towner, S et al., (2004). Rapid diagnosis of Ebola hemorrhagic fever by reverse transcription-PCR in an outbreak setting and assessment of patient viral load as a predictor of outcome. Journal of virology, 78(8), pp. 4330–4341.

43. Zhao, G. (2007). SARS molecular epidemiology: a Chinese fairy tale of controlling an emerging zoonotic disease in the genomics era. Philosophical Transactions of the Royal Society B: Biological Sciences, 362(1482), pp. 1063–1081.
44. Paquette. S. G et al., (2015). Influenza transmission in the mother-infant dyad leads to severe disease, mammary gland infection, and pathogenesis by regulating host responses. PLoS pathogens, 11(10), p. e1005173.
45. Chunduri, S., Ghaffari, M., Lahijani, M. S., Srinivasan, A., & Namilae, S. (2018, May). Parallel low discrepancy parameter sweep for public health policy. In 2018 18th IEEE/ACM International Symposium on Cluster, Cloud and Grid Computing (CCGRID) (pp. 291-300). IEEE.
46. Radović, I., Tichy, R. F., & Sobol, I. M. (1996). Quasi-Monte Carlo methods for numerical integration: Comparison of different low discrepancy sequences. Monte Carlo Methods and Applications, 2(1), 1-14.
47. Morokoff, W. J., & Caflisch, R. E. (1994). Quasi-random sequences and their discrepancies. SIAM Journal on Scientific Computing, 15(6), 1251-1279.
48. Göncü, A. (2009). Monte Carlo and quasi-Monte Carlo methods in financial derivative pricing.(PhD thesis)
49. Halton, J. H. (1964). Algorithm 247: Radical-inverse quasi-random point sequence. Communications of the ACM, 7(12), 701-702.
50. Cools, R. (2002). Advances in multidimensional integration. Journal of computational and applied mathematics, 149(1), 1-12.

51. Sen, S. K., Samanta, T., & Reese, A. (2006). Quasi-versus pseudo-random generators: discrepancy, complexity and integration-error based comparison. International Journal of Innovative Computing, Information and Control, 2(3), 621-651.
52. Bender, G. (2016). Airport Terminal Security Screening Checkpoints: Still An Industrial Engineering Problem. Retrieved from https://www.arenasimulation.com/blog/post/airport-terminal-security-screening-checkpoints-still-an-industrial-engineer.